JACS
JOURNAL OF THE AMERICAN CHEMICAL SOCIETY

Communication

pubs.acs.org/JACS

How "Hollow" Are Hollow Nanoparticles?

Paul Podsiadlo,[†] Soon Gu Kwon,[†] Bonil Koo,[†] Byeongdu Lee,[‡] Vitali B. Prakapenka,[§] Przemyslaw Dera,[§,‡] Kirill K. Zhuravlev,[§] Galyna Krylova,[†] and Elena V. Shevchenko*[,†]

[†]Center for Nanoscale Materials and [‡]Advanced Photon Source, Argonne National Laboratory, Argonne, Illinois 60439, United States
[§]Center of Advanced Radiation Sources, University of Chicago, Argonne, Illinois 60439, United States

Supporting Information

ABSTRACT: Diamond anvil cell (DAC), synchrotron X-ray diffraction (XRD), and small-angle X-ray scattering (SAXS) techniques are used to probe the composition inside hollow γ-Fe_3O_4 nanoparticles (NPs). SAXS experiments on 5.2, 13.3, and 13.8 nm hollow-shell γ-Fe_3O_4 NPs, and 6 nm core/14.8 nm hollow-shell Au/Fe_3O_4 NPs, reveal the significantly high (higher than solvent) electron density of the void inside the hollow shell. In high-pressure DAC experiments using Ne as pressure-transmitting medium, formation of nanocrystalline Ne inside hollow NPs is not detected by XRD, indicating that the oxide shell is impenetrable. Also, FTIR analysis on solutions of hollow-shell γ-Fe_3O_4 NPs fragmented upon refluxing shows no evidence of organic molecules from the void inside, excluding the possibility that organic molecules get through the iron oxide shell during synthesis. High-pressure DAC experiments on Au/Fe_3O_4 core/hollow-shell NPs show good transmittance of the external pressure to the gold core, indicating the presence of the pressure-transmitting medium in the gap between the core and the hollow shell. Overall, our data reveal the presence of most likely small fragments of iron and/or iron oxide in the void of the hollow NPs. The iron oxide shell seems to be non-porous and impenetrable by gases and liquids.

Recent progress in colloidal synthesis has resulted in the discovery of nanoparticles (NPs) with different morphologies, including dumbbells,[1] tetrapods,[2] octapods,[3] nanorings,[4] hollow NPs,[5] and core/hollow shells.[6] Among them, hollow NPs are of special interest because of their unique magnetic, catalytic, optical, and electrochemical properties.[7] They can also serve as carriers for controllable drug release.[8] Hollow NPs can be formed by galvanic replacement reactions[9] or by the Kirkendall effect as a result of oxidation of metal NPs.[5a,14] The difference in the diffusion rates of oxygen and metal atoms moving in opposite directions during oxidation results in vacancies that condense inside the NPs and form a void. Besides the importance of the composition inside hollow NPs for practical applications, there is a fundamental question: How "hollow" are hollow NPs? We propose use of a diamond anvil cell (DAC) technique to probe the composition inside hollow NPs and analyze the penetrability of their inorganic shells. We systematically analyze differently sized hollow iron oxide NPs with and without gold or iron cores, as examples, using DAC combined with synchrotron X-ray diffraction (XRD) and small-angle X-ray scattering (SAXS).

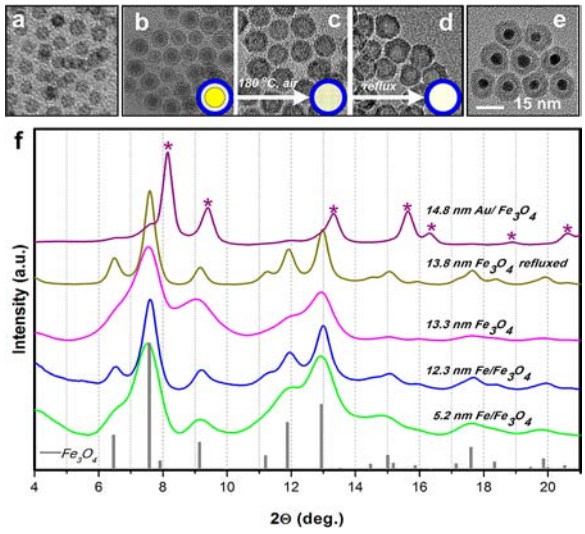

Figure 1. TEM overview of as-synthesized (a) 5.2 nm hollow Fe_3O_4 NPs, (b) 12.3 nm hollow Fe_3O_4 NPs with 6.5 nm Fe cores, (c) 13.3 nm hollow NPs obtained by oxidizing the NPs shown in panel b, (d) 13.8 nm hollow Fe_3O_4 NPs obtained by refluxing the NPs in panel c at 298 °C, and (e) Fe_3O_4 hollow NPs with encapsulated 6 nm Au NPs. (f) Summary of XRD data at ambient pressure. Indexing of Fe_3O_4 and Au is depicted as gray lines and purple stars, respectively.

Hollow iron oxide NPs were obtained upon oxidation of iron NPs in an octadecene solution by air flow at 180 °C.[5d,6c] Iron atoms diffuse out of NPs faster than oxygen atoms diffuse in from the surface of NPs, forming cation vacancies that coalesce to form voids inside the NPs. In this study we investigated 5.2 and 13.3 nm hollow Fe_3O_4 NPs, with shell thicknesses of ~1.7 and ~2.3 nm, respectively (Figure 1). As evidenced by broad diffraction peaks (Figure 1f), the iron oxide shell is very polycrystalline, in agreement with previously published transmission electron microscopy (TEM) data.[5d,6c] According to synchrotron XRD analysis, the crystalline structure of hollow iron oxide NPs was identified as γ-Fe_3O_4 (Figure 1) in all studied samples, similar to the previously published data.[5c] A significant improvement in the crystallinity of the larger hollow NPs was observed as a result of refluxing at 298 °C, as indicated by the sharpening of the diffraction peaks (Figure 1f). Improvement in crystallinity upon refluxing was also previously observed by Peng et al.[5c,8b] However, refluxing of 5.2 nm hollow Fe_3O_4 NPs resulted in

Received: December 6, 2012
Published: January 29, 2013

dx.doi.org/10.1021/ja311926r | J. Am. Chem. Soc. 2013, 135, 2435−2438

Table 1. Summary of the Parameters Used in Simulations of Experimental SAXS Results Shown in Figure 2

					electron density (e/Å^3)			
sample	core	void radius (Å)	core−shell distance (Å)	shell thickness (Å)	core	void	shell	solvent
5.2 nm Fe_3O_4 hollow shell	n/a	9.6 ± 3.4	n/a	16.8	n/a	0.1905		
12.3 nm Fe/Fe_3O_4 core/hollow shell	Fe	33.4 ± 9.0	16.8	11.1	2.16	1.077		
13.3 nm Fe_3O_4 hollow shell	n/a	43.8 ± 4.9	n/a	22.7	n/a	0.774	1.4898	0.2836
13.8 nm Fe/Fe_3O_4 hollow shell (refluxed)	n/a	39.1	n/a	29.7	n/a	0.436		
14.8 nm Au/Fe_3O_4 core/hollow shell	Au	29.9	16.1	27.7	4.66	0.7659		

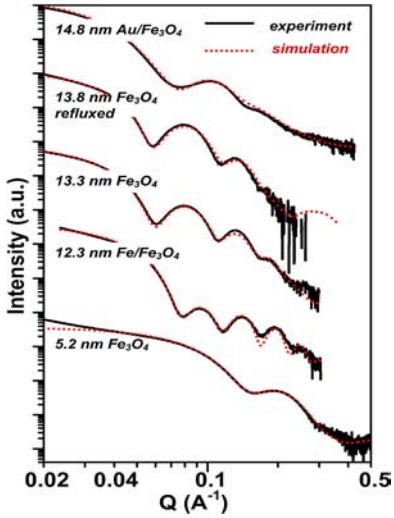

Figure 2. SAXS spectra of NPs dispersed in toluene, and computer simulation fits obtained using parameters shown in Table 1.

their fragmentation (Figure S1). Similar to the previous studies,[5c] we observed no diffraction peaks from pure Fe core before and after refluxing (Figure 1).

Given the current understanding of the structural/chemical composition of hollow NPs formed via the Kirkendall effect,[5a,10] the interior part of the hollow NPs, formed during coalescence of diffusing vacancies, should potentially be a vacuum or can be filled with solvent and some original component of the NPs before oxidation (i.e., metal), depending on whether the shell is porous. For example, Yin et al. suggested that the shell of Co/CoO core/hollow-shell NPs can have as much as 15 vol% porosity,[5b] which might explain the ability of ethylene to diffuse into the interior of Pt/CoO core/hollow-shell NCs and participate in the hydrogenation reaction.[5a] As such, porosity of the shell may also allow other materials, e.g., solvents, oxidizing agent, or reaction precursors, to penetrate inside the NPs. Previously it was reported that thermal annealing of 16 nm Fe_3O_4 hollow NPs can form ∼2 nm pores in the shell, clearly visible by TEM.[8b] However, their complete opening inside the hollow NPs was achieved only upon acid treatment of the NPs.

To probe the internal composition of hollow NPs, we first performed SAXS measurements at ambient conditions on different types of hollow Fe_3O_4 NPs dispersed in toluene (Figure 2). Scattering patterns with known form factors are typically used to estimate the size and shape distributions of NPs from their compositional information in terms of electron density (number of electrons per unit volume). Simulations of the patterns based on known chemistry of the shell and the solid core allowed optimizing their thickness and radius as well as electron density of the hollow interior.[11] Figure 2 compiles the scattering patterns and the simulated curves for all of the NP types, and Table 1 summarizes the parameters used to fit experimental data. Altogether, the structural parameters obtained in the simulations fit surprisingly well with the values obtained from TEM. Based on the fact that the void inside the hollow NPs is a result of coalescence of vacancies, we should expect zero electron density in the hollow interior. However, simulation results showed significantly higher electron density (Figure 1). Thus, NPs called "hollow" are unlikely to be empty.

Simulation of the SAXS data (Figure 2) shows that 5.2 nm hollow Fe_3O_4 NPs have the lowest electron density among all studied samples (Table 1), and the electron density of the inner part of 5.2 nm hollow NPs is lower than that of the organic solvent. In the case of as-synthesized larger hollow-shell NPs, electron density of the interior void is substantial. In fact, it is intermediate between those of the pure solvent and solid Fe_3O_4. The 12.3 nm core/hollow-shell NPs showed high electron density in the void between the core and the shell (Table 1), indicating the presence of inorganic material in the area that looks like a gap between the core and the shell on TEM images. We assumed that the small remnants of pure Fe or iron oxide remained inside the hollow cavity in the form of fine whiskers or dispersed fine clusters. This assumption seems to be very reasonable since we observe the highest electron density in the void of the core/hollow-shell Fe/Fe_3O_4 NPs. The presence of the bridges that serve as "pipelines" for diffusion of metal cations to the NP surface during the oxidation process was previously observed in Fe/Fe_3O_4 and Co/CoO NPs.[5a,c,d] The presence of small fragments of iron within the hollow void is also supported by the decrease of the electron density inside the hollow NPs upon refluxing, associated with the increase of the oxide shell thickness (Figure 2, Table 1).

In order to investigate the penetrability of the inorganic oxide shell for the gas molecules and to further analyze the composition of the interior void in hollow NPs, we performed high-pressure synchrotron XRD experiments. The 13.3 nm Fe_3O_4 NPs have the largest "empty void" inside; thus, they can be expected to accumulate the most foreign material. The 13.3 nm Fe_3O_4 NPs were loaded into the DAC using Ne as a pressure-transmitting medium. Under pressure, liquid and gas solidify, forming crystalline or amorphous phases. XRD analysis under high pressure can reveal crystallized materials that were in gas or liquid phases at ambient conditions. In the case of porous shells, Ne might penetrate inside the hollow Fe_3O_4 shell and crystallize in nanometer sizes that will lead to the appearance of broad signals characteristic of nanocrystals. We compared the widths of the diffraction lines corresponding to crystalline Ne in three samples: Ne without NPs, solid 13.5 nm Fe_3O_4 NPs, and hollow 13.3 nm Fe_3O_4 NPs. (Note that since Ne is a pressure-transmitting medium, the signal corresponding to it will always be present.) The 2D XRD patterns revealed only sharp lines of "bulk" Ne (Figure 3). No diffuse, broad lines characteristic of nanosized Ne were found. Thus we can rule out the penetrability of the oxide shells by the molecules of Ne and hence conclude that hollow iron oxide NPs do not have pores or structural defects that allow

dx.doi.org/10.1021/ja311926r | J. Am. Chem. Soc. 2013, 135, 2435−2438

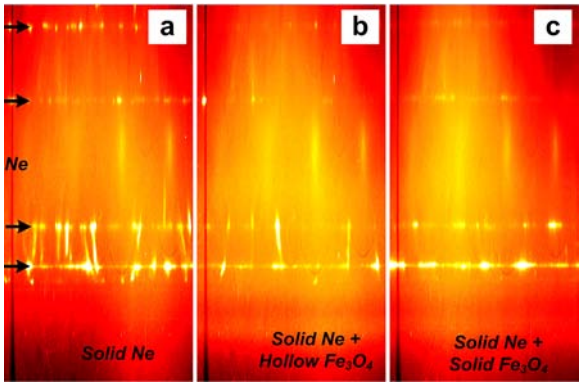

Figure 3. 2D diffraction patterns of Ne (a), hollow iron oxide NPs (b), and solid iron oxide NPs at 37.0(4) GPa. Ne was used as a pressure-transmitting medium, but no diffuse broad signals characteristic of nanosized Ne are seen.

the diffusion of gas. Also, no peaks corresponding to new materials were observed at any pressure, ruling out the presence of crystalline organic phase inside the hollow iron oxide shell; however, at this point we cannot exclude the presence of amorphous organic materials.

The presence of material inside the hollow NPs that can transmit external pressure to the core was also confirmed in our high-pressure experiments on hollow Fe_3O_4 NPs encapsulating a 6 nm Au core (Figure 4). Note that Au is standard for pressure calibration due to the linear dependence of its unit cell volume on pressure in a very broad pressure range.[12] The XRD pattern of the Au/Fe_3O_4 NPs at atmospheric pressure showed very strong diffraction from Au core (Figures 1f and 4). We wanted to see whether, under high external pressure, the seemingly empty space between the Au core and the Fe_3O_4 shell would transmit force to the Au core (Figure 1e). At one extreme, lack of force transmission, e.g., in the case of the void containing a vacuum, should result in a lack of observable compression of the Au core, and there should be no shifts in the XRD pattern. At the other extreme, i.e., when the void is filled with material, the pressure should be transmitted to the core, and XRD should reveal shifts reflecting compression of the Au core.[12] We can exclude fragmentation of the hollow iron oxide shell since SAXS patterns of 13.3 nm hollow Fe_3O_4 before and after compression up to 51.(8) GPs are identical, meaning that the morphology of hollow NPs was preserved during compression and pressure release (Figure S4). We found that the Au core was significantly compressible, although not as much as bulk Au.[12] However, Au NPs have been previously found to have a significantly elevated bulk modulus,[13] which can also account for decreased compressibility in our case. The bulk modulus of bulk gold is B_0 = 170 GPa,[12] while 50−100 nm Au NPs have been reported to have B_0 = 210 GPa,[14] and B_0 = 290 GPa has been obtained for 30 nm NPs.[13] Fitting the XRD data (Figure 4b) with both Vinet and Birch−Murnaghan (B-M) equation of states (EOS)[12] gave consistent results. Thus, a bulk modulus of B_0 = 215 GPa was obtained for our 6 nm Au NPs encapsulated inside hollow Fe_3O_4 shells using the pressure derivative of the bulk modulus, B_0', fixed to 4.0 (allowing us to reduce third-order B-M EOS to the second-order one) and zero-pressure volume V_0 = 67.1(1) GPa. As in the case of hollow 13.3 nm Fe_3O_4 NPs, no peaks corresponding to the nanosized Ne were found (Figure 4a). Thus, compressibility of Au NPs encapsulated inside the hollow iron oxide shell under

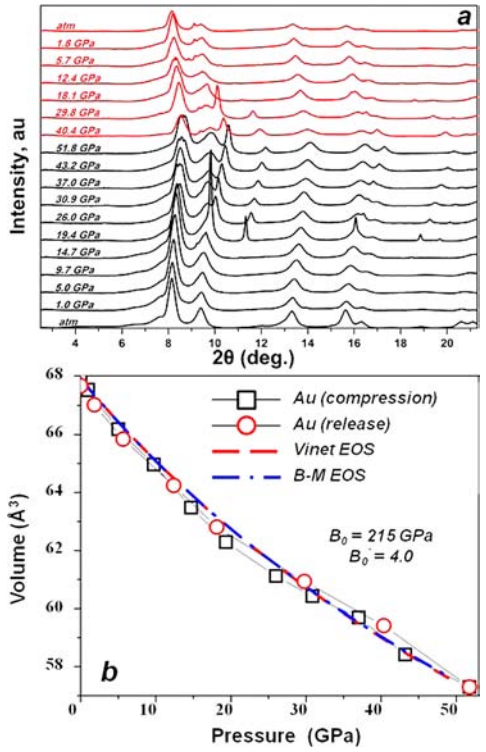

Figure 4. (a) Pressure-dependent XRD compression and release spectra up to 51.(8) GPa for Au/Fe_3O_4 core/hollow-shell NPs. Sharp peaks observed in pressure range of 9.7−51.8 GPa correspond to solid Ne. (b) Calculation of bulk modulus of the Au core from fitting of the Birch−Murnaghan and Vinet's equations of state to the XRD data.

applied external pressure confirms the presence of a pressure-transmitting medium different than Ne inside the hollow NPs.

The composition of the internal void inside of the hollow-shell NPs was further investigated using FTIR. Upon refluxing in benzyl ether at 298 °C under air flow (12.5 mL/min) for 1 h, 5.2 nm hollow Fe_3O_4 NPs and 12.3 nm Fe/Fe_3O_4 core/hollow-shell NPs broke into fragments, which would release the possible content of the hollow NPs to the solution, while no fragmentation of 13.3 nm hollow NPs was observed. Comparative analysis of the supernatant solutions obtained by complete precipitation of inorganic material in these three samples allows tracing the presence of organic materials that can be potentially encapsulated within the hollow NPs during the synthesis or post-preparative treatments and thus are not crystallized upon compression. Before refluxing, each sample was washed with the same amount of non-solvents (e.g., acetone and methanol) and re-dissolved in 10 mL of benzyl ether (note that hollow NPs were synthesized in octadecene). After refluxing, equivalent amounts of non-solvents were added into the NP solutions, followed by centrifugation (8000 rpm for 1 min). The supernatant solutions after centrifugation were concentrated by evaporation of methanol and acetone and analyzed by FTIR (Figures S2 and S3). Similarity among the FTIR spectra of all as-synthesized and refluxed samples (Figure S3) suggests that organic materials did not penetrate into the interior part of the NPs during the synthesis or post-preparative procedures.

In conclusion, our data underscore the presence of pressure-transmitting material inside the Fe_3O_4 hollow NPs. Taking into account (i) the high electron density of internal void in hollow NPs, as evidenced by SAXS data; (ii) the absence of gaseous and/or liquid compounds within this void, as evidenced by FTIR and

dx.doi.org/10.1021/ja311926r | J. Am. Chem. Soc. 2013, 135, 2435−2438

high-pressure experiments; and (iii) the transmittance of pressure to the core material from the external force, as observed in our experiments with Au core/Fe_3O_4 hollow-shell NPs (Figure 4), we can assume that tiny remnants of amorphous iron and/or iron oxide that cannot be detected by TEM or XRD techniques are very likely to be present within the internal void of hollow Fe_3O_4 NPs. Polycrystalline Fe_3O_4 shells are unlikely to contain pores since diffusion of small gas molecules was not observed. Prolonged oxidative refluxing of the relatively large (>12 nm) Fe_3O_4 NPs allows partial annealing of the remnants within the void.

Core/hollow-shell geometry is very attractive for the design of catalysts since the hollow shell prevents sintering of the catalytically active core; thus, knowledge about the composition of the voids inside hollow structures and penetrability of the hollow shell is critical. We believe that our approach toward analysis of the void composition of hollow Fe_3O_4 NPs can be used to study penetrability of any type of nanoshells and allows compositional analysis of the inner voids of any hollow nanostructures.

■ ASSOCIATED CONTENT

Ⓢ Supporting Information

Details on synthesis; TEM images; and SAXS, FTIR, and pressure error data. This material is available free of charge via the Internet at http://pubs.acs.org.

■ AUTHOR INFORMATION

Corresponding Author

eshevchenko@anl.gov

Notes

The authors declare no competing financial interest.

■ ACKNOWLEDGMENTS

Work at the Center for Nanoscale Materials and use of the Advanced Photon Source was supported by the Office of Science, Office of Basic Energy Sciences, of the U.S. Department of Energy under Contract No. DE-AC02-06CH11357. P.P. acknowledges support from the Willard Frank Libby postdoctoral fellowship from Argonne National Laboratory. GeoSoilEnviroCARS is supported by the National Science Foundation—Earth Sciences (EAR-0622171) and Department of Energy—Geosciences (DE-FG02-94ER14466).

■ REFERENCES

(1) (a) Wang, C.; Daimon, H.; Sun, S. *Nano Lett.* **2009**, *9*, 1493. (b) Yu, H.; Chen, M.; Rice, P. M.; Wang, S. X.; White, R. L.; Sun, S. *Nano Lett.* **2005**, *5*, 379. (c) Kwon, K. W.; Shim, M. *J. Am. Chem. Soc.* **2005**, *127*, 10269. (d) Pellegrino, T.; Fiore, A.; Carlino, E.; Giannini, C.; Cozzoli, P. D.; Ciccarella, G.; Respaud, M.; Palmirotta, L.; Cingolani, R.; Manna, L. *J. Am. Chem. Soc.* **2006**, *128*, 6690. (e) Gu, H.; Zheng, R.; Zhang, X.; Xu, B. *J. Am. Chem. Soc.* **2004**, *126*, 5664. (f) Gu, H.; Yang, Z.; Gao, J.; Chang, C. K.; Xu, B. *J. Am. Chem. Soc.* **2005**, *127*, 34. (g) Krylova, G.; Dimitrijevic, N. M.; Talapin, D. V.; Guest, J. R.; Borchert, H.; Lobo, A.; Rajh, T.; Shevchenko, E. V. *J. Am. Chem. Soc.* **2010**, *132*, 9102. (h) Krylova, G.; Giovanetti, L. J.; Requejo, F. G.; Dimitrijevic, N. M.; Prakapenka, A.; Shevchenko, E. V. *J. Am. Chem. Soc.* **2012**, *134*, 4384. (i) Wu, H.; Chen, O.; Zhuang, J.; Lynch, J.; LaMontagne, D.; Nagaoka, Y.; Cao, Y. C. *J. Am. Chem. Soc.* **2011**, *133*, 14327.

(2) (a) Manna, L.; Milliron, D. J.; Meisel, A.; Scher, E. C.; Alivisatos, A. P. *Nat. Mater.* **2003**, *2*, 382. (b) Manna, L.; Scher, E. C.; Alivisatos, A. P. *J. Am. Chem. Soc.* **2000**, *122*, 12700. (c) Liu, H.; Alivisatos, A. P. *Nano Lett.* **2004**, *4*, 2397. (d) Djurii, A. B.; Choy, W. C. H.; Roy, V. A. L.; Leung, Y. H.; Kwong, C. Y.; Cheah, K. W.; Rao, T. K. G.; Chan, W. K.; Lui, H. F.; Surya, C. *Adv. Funct. Mater.* **2004**, *14*, 856. (e) Cozzoli, P. D.; Snoeck, E.; Garcia, M. A.; Giannini, C.; Guagliardi, A.; Cervellino, A.; Gozzo, F.; Hernando, A.; Achterhold, K.; Ciobanu, N.; Parak, F. G.; Cingolani, R.; Manna, L. *Nano Lett.* **2006**, *6*, 1966. (f) Fiore, A.; Mastria, R.; Lupo, M. G.; Lanzani, G.; Giannini, C.; Carlino, E.; Morello, G.; Giorgi, M. D.; Li, Y.; Cingolani, R.; Manna, L. *J. Am. Chem. Soc.* **2009**, *131*, 2274.

(3) (a) Chou, S. W.; Zhu, C. L.; Neeleshwar, S.; Chen, C. L.; Chen, Y. Y.; Chen, C. C. *Chem. Mater.* **2009**, *21*, 4955. (b) Ren, J.; Tilley, R. D. *J. Am. Chem. Soc.* **2007**, *129*, 3287. (c) Deka, S.; Miszta, K.; Dorfs, D.; Genovese, A.; Bertoni, G.; Manna, L. *Nano Lett.* **2010**, *10*, 3770. (d) Huang, X.; Zhao, Z.; Fan, J.; Tan, Y.; Zheng, N. *J. Am. Chem. Soc.* **2011**, *133*, 4718.

(4) (a) Cho, K. S.; Talapin, D. V.; Gaschler, W.; Murray, C. B. *J. Am. Chem. Soc.* **2005**, *127*, 7140. (b) Hu, M. J.; Lu, Y.; Zhang, S.; Guo, S. R.; Lin, B.; Zhang, M.; Yu, S. H. *J. Am. Chem. Soc.* **2008**, *130*, 11606. (c) Guo, Q.; Kim, S. J.; Kar, M.; Shafarman, W. N.; Birkmire, R. W.; Stach, E. A.; Agrawal, R.; Hillhouse, H. W. *Nano Lett.* **2008**, *8*, 2982. (d) Jia, C. J.; Sun, L. D.; Luo, F.; Han, X. D.; Heyderman, L. J.; Yan, Z. G.; Yan, C. H.; Zheng, K.; Zhang, Z.; Takano, M.; Hayashi, N.; Eltschka, M.; Kläui, M.; Rüdiger, U.; Kasama, T.; Cervera-Gontard, L.; Dunin-Borkowski, R. E.; Tzvetkov, G.; Raabe, J. *J. Am. Chem. Soc.* **2008**, *130*, 16968.

(5) (a) Yin, Y.; Rioux, R. M.; Erdonmez, C. K.; Hughes, S.; Somorjai, G. A.; Alivisatos, A. P. *Science* **2004**, *304*, 711. (b) Yin, Y.; Erdonmez, C. K.; Cabot, A.; Hughes, S.; Alivisatos, A. P. *Adv. Funct. Mater.* **2006**, *16*, 1389. (c) Peng, S.; Sun, S. *Angew. Chem., Int. Ed.* **2007**, *46*, 4155. (d) Cabot, A.; Puntes, V. F.; Shevchenko, E.; Yin, Y.; Balcells, L.; Marcus, M. A.; Hughes, S. M.; Alivisatos, A. P. *J. Am. Chem. Soc.* **2007**, *129*, 10358. (e) An, K.; Kwon, S. G.; Park, M.; Na, H. B.; Baik, S. I.; Yu, J. H.; Kim, D.; Son, J. S.; Kim, Y. W.; Song, I. C.; Moon, W. K.; Park, H. M.; Hyeon, T. *Nano Lett.* **2008**, *8*, 4252. (f) Hung, L. I.; Tsung, C. K.; Huang, W.; Yang, P. *Adv. Mater.* **2010**, *22*, 1910. (g) Piao, Y.; Kim, J.; Na, H. B.; Kim, D.; Baek, J. S.; Ko, M. K.; Lee, J. H.; Shokouhimehr, M.; Hyeon, T. *Nat. Mater.* **2008**, *7*, 242.

(6) (a) Sun, Y.; Wiley, B.; Li, Z. Y.; Xia, Y. *J. Am. Chem. Soc.* **2004**, *126*, 9399. (b) Kim, M.; Sohn, K.; Na, H. B.; Hyeon, T. *Nano Lett.* **2002**, *2*, 1383. (c) Shevchenko, E. V.; Bodnarchuk, M. I.; Kovalenko, M. V.; Talapin, D. V.; Smith, R. K.; Aloni, S.; Heiss, W.; Alivisatos, A. P. *Adv. Mater.* **2008**, *20*, 4323. (d) Yeo, K. M.; Shin, J.; Lee, I. S. *Chem. Commun.* **2010**, 64.

(7) (a) Wang, X.; Fu, H.; Peng, A.; Zhai, T.; Ma, Y.; Yuan, F.; Yao, J. *Adv. Mater.* **2009**, *21*, 1636. (b) Levin, C. S.; Hofmann, C.; Ali, T. A.; Kelly, A. T.; Morosan, E.; Nordlander, P.; Whitmire, K. H.; Halas, N. J. *ACS Nano* **2009**, *3*, 1379. (c) Kim, S. W.; Kim, M.; Lee, W. Y.; Hyeon, T. *J. Am. Chem. Soc.* **2002**, *124*, 7642. (d) Mahmoud, M. A.; Saira, F.; El-Sayed, M. A. *Nano Lett.* **2010**, *10*, 3764. (e) Wu, S. H.; Tseng, C. T.; Lin, Y. S.; Lin, C. H.; Hung, Y.; Mou, C. Y. *J. Mater. Chem.* **2011**, *21*, 789. (f) Jain, P. K.; El-Sayed, M. A. *J. Phys. Chem. C* **2007**, *111*, 17451. (g) Lou, X. W. D.; Archer, L. A.; Yang, Z. *Adv. Mater.* **2008**, *20*, 3987. (h) Liu, J.; Qiao, S. Z.; Chen, J. S.; Lou, X. W.; Xing, X.; Lu, G. Q. *Chem. Commun.* **2011**, 12578. (i) Koo, B.; Xiong, H.; Slater, M. D.; Prakapenka, V. B.; Balasubramanian, M.; Podsiadlo, P.; Johnson, C. S.; Rajh, T.; Shevchenko, E. V. *Nano Lett.* **2012**, *12*, 2429.

(8) (a) Hu, S. H.; Chen, S. Y.; Liu, D. M.; Hsiao, C. S. *Adv. Mater.* **2008**, *20*, 2690. (b) Cheng, K.; Peng, S.; Xu, C.; Sun, S. *J. Am. Chem. Soc.* **2009**, *131*, 10637. (c) Hao, R.; Xing, R.; Xu, Z.; Hou, Y.; Gao, S.; Sun, S. *Adv. Mater.* **2010**, *22*, 2729. (d) An, K.; Hyeon, T. *Nano Today* **2009**, *4*, 359.

(9) (a) Sun, Y.; Xia, Y. *Science* **2002**, *298*, 2176. (b) Yin, Y.; Erdonmez, C.; Aloni, S.; Alivisatos, A. P. *J. Am. Chem. Soc.* **2006**, *128*, 12671.

(10) Fan, H. J.; Gösele, U.; Zacharias, M. *Small* **2007**, *3*, 1660.

(11) Roe, R. J. *Method of X-ray and Neutron Scattering in Polymer Science*; Oxford University Press: Oxford, UK, 2000.

(12) Fei, Y.; Ricolleau, A.; Frank, M.; Mibe, K.; Shen, G.; Prakapenka, V. *Proc. Natl. Acad. Sci. U.S.A.* **2007**, *104*, 9182.

(13) Gu, Q. F.; Krauss, G.; Steurer, W.; Gramm, F.; Cervellino, A. *Phys. Rev. Lett.* **2008**, *100*, 045502.

(14) Martin, C. D.; Antao, S. M.; Chupas, P. J.; Lee, P. L.; Shastri, S. D.; Parise, J. B. *Appl. Phys. Lett.* **2005**, *86*, 061910.